JOURNAL of the MEXICAN CHEMICAL SOCIETY

https://www.jmcs.org.mx/

Article

Open Access

J. Mex. Chem. Soc. **2026**, *70(1):e2436*

Received January 27th, 2025
Accepted November 28th, 2025

http://dx.doi.org/10.29356/jmcs.v70i1.2436
e-location ID: 2436

Keywords:
TiO_2; nanoparticles; photocatalyst; bipyramidal; Congo red dye

Palabras clave:
TiO_2, nanopartículas; fotocatálisis; bipirámide; colorante rojo Congo

***Corresponding author:**
Edgar-Alonso Reynoso-Soto
email: edgar.reynoso@tectijuana.edu.mx

©2026, edited and distributed by Sociedad Química de México

ISSN-e 2594-0317

Synthesis of Octahedral Bipyramid TiO_2 Nanoparticles Free of Growth Agent as Congo Red Photocatalyst

Paulina Vargas-Rodriguez[1], Carla Marlene Toledo Bonola[1], Carolina Silva-Carrillo[2], Brenda Cecilia Alcantar-Vazquez[3], Rosa-María Félix-Navarro[1], Rosalio Velarde-Barraza[1], Edgar-Alonso Reynoso-Soto[1*]

[1]Tecnológico Nacional de México/Instituto Tecnológico de Tijuana, Blvd Alberto Limón Padilla y AV. ITR Tijuana S/N Colonia Mesa de Otay CP: 22500, Tijuana BC, México.
[2]Facultad de Ciencias Químicas e Ingeniería, Universidad Autónoma de Baja California. Clzd. Universidad No. 14418, parque internacional industrial CP: 22390, Tijuana BC, México.
[3]Instituto de Ingeniería, Universidad Nacional Autónoma de México. Av. Universidad 3000, Coyoacán, C.P. 04510, Ciudad de México, México.

Abstract. In this work, we prepared anatase TiO_2 nanoparticles with octahedral bipyramidal shapes with different (001)/(101) ratio facets as photocatalysts for Congo red (CR) dye. The general method to prepare such nano-TiO_2 photocatalysts involves a peptization step with HNO_3 and hydrothermal treatment at different temperatures, making this a facile and friendly method to controllably synthesize TiO_2 with octahedral bipyramidal shape and tuned (001)/(101) ratio free of capping surfactants or direction agent like HF. The photocatalytic activity of these anatase TiO_2 nanoparticles was evaluated through CR dye photodegradation under UV light illumination. It was shown that all samples can present a photocatalytic activity, and the degradation efficiency and kinetics depend on nanoparticle size and (001)/(101) ratio facets.

Resumen. En este trabajo preparamos nanopartículas de TiO_2 anatasa con forma bipiramidal octaédrica con diferentes facetas de proporción (001)/(101) como fotocatalizadores para el colorante Congo rojo (CR). El método general para

©2026, Sociedad Química de México. Authors published within this journal retain copyright and grant the journal right of first publication with the work simultaneously licensed under a Creative Commons Attribution License that enables reusers to distribute, remix, adapt, and build upon the material in any medium or format for noncommercial purposes only, and only so long as attribution is given to the creator.

J. Mex. Chem. Soc. **2026**, *70(1):e2436*
Regular Issue
©2026, Sociedad Química de México
ISSN-e 2594-0317

preparar dichos nano-fotocatalizadores de TiO_2 implica un paso de peptización con HNO_3 y un tratamiento hidrotermal a diferentes temperaturas, lo que hace de este un método fácil y amigable para sintetizar de manera controlada TiO_2 con forma bipiramidal octaédrica y proporción ajustada (001)/(101) libre de surfactantes de recubrimiento o agentes de dirección como HF. La actividad fotocatalítica de estas nanopartículas de TiO_2 anatasa se evaluó a través de la fotodegradación del colorante RC bajo iluminación de luz UV. Se demostró que todas las muestras pueden presentar una actividad fotocatalítica y la eficiencia de degradación y la cinética dependen del tamaño de las nanopartículas y de la proporción de facetas (001)/(101).
Palabras clave: TiO_2, nanopartículas; fotocatálisis; bipirámide; colorante rojo Congo.

Introduction

Studies on wastewater treatment have focused on developing suitable technologies for removing organic pollutants, such as wet oxidation, biological oxidation, electrochemical redox, and advanced oxidation processes (AOPs).[1] Photocatalysis is one of the most efficient AOP methods for degrading organic compounds in water. The photocatalytic oxidation process studies are focused on understanding its mechanisms or kinetics because its principal degradation mechanism route goes by the hydroxyl radical *OH formed on the photocatalyst surface under UV radiation.[2]

The development of advanced photocatalysts to resolve water pollution problems is becoming a focal point in this century. Nanostructured photocatalyst materials have been attracting significant attention due to their desirable properties, including high selectivity, easy separation, recyclability, solubility, large-scale applicability, cost-effectiveness, and reproducibility.[3] Several materials and composites were used as photocatalysts, including carbon nanomaterials with metallic oxide and metallic oxides like Fe_2O_3, ZnO, WO_3, and TiO_2, to improve the degradation of pollutants.[4]

Titania (TiO_2) is a semiconductor material that has received a broad range of applications thanks to its intriguing physical and chemical properties and cheap, abundant, and nontoxic nature.[5] TiO_2 has long been investigated for its potential use as a photocatalyst among the three major crystal phases: rutile, anatase, and brookite. Anatase has demonstrated the most effective photocatalytic performance, and the activity may be improved by controlling the following factors: crystallinity, doping, surface defects, increasing active surface area, and controlling exposed facets.[6]

The TiO_2 facet engineering has attracted significant research interest in the past decade. The Wulff construction model predicted anatase shape: a slightly truncated bipyramid enclosed with 94 % of (101) and fewer 6 % (001) facets.[7] Although high-performance TiO_2 materials can be finely tuned through their surface and interface properties, some vital issues still need to be carefully considered shortly. For example, the generality of facet-dependent properties for a wide range of facets with different materials and the influence of surface reconstruction on the performance of micro- or nanosized facets. Therefore, the synthesis of well-defined anatase TiO_2 with considerable exposure to photoactive (001) facets has attracted particular interest. For example, Yang et al. have successfully synthesized anatase TiO_2 single crystals with 47 % surface exposing (001) facets using HF as the morphology controlling agent.[8] Different precursors for TiO_2 synthesis have significant effects on the nanocrystals morphology and constitution, like the dissolvable titanium salt including TiF_4,[9] $Ti(SO_4)_2$,[10] $TiCl_4$,[11] $Ti(OBu)_4$,[12] and $Ti\{OCH(CH_3)_2\}_4$,[13] it is hard to control the crystal growing process, which led to the size of TiO_2 with (001) facets crystals larger.

Dyes are organic compounds based on aromatic structures that consist of conjugated planar ring systems accompanied by delocalized Π electron clouds and are used for coloring applications in several modern industries such as textile, leather, paper, printing, paint, pigments, rubber, and plastic.[14] Organic dyes bearing an azo group (−N=N−) are known as azo dyes and have commercial uses in the textile, leather, and food industries. These dyes have been divided into two types, based on their charge: cationic and anionic azo dyes.[15] The wastewater containing organic dye pollutants blocks the ecosystem and causes threats to environmental sustainability, which is persistent due to the poor biodegradability of these dyes. Dyes absorb the visible spectrum light from 380 to 750 nm.[16]

http://dx.doi.org/10.29356/jmcs.v70i1.2436

J. Mex. Chem. Soc. **2026**, *70(1):e2436*
Regular Issue
©2026, Sociedad Química de México
ISSN-e 2594-0317

Congo Red (diazo dye) is recognized as a carcinogen compound because it contains an aromatic amine in its structure. The presence of aromatic structures makes azo dyes resistant to natural degradation. Dyes remain in the environment for an extended period, adversely affecting the fauna and flora.[17] Photocatalytic decomposition of Congo red dye has been studied using expensive photocatalysts such as polypyrrole/silver/graphene nanocomposite, chitosan/SnO_2 nanocomposite, TiO_2-doped cobalt ferrite nanoparticles, chitosan/Fe_3O_4 nanocomposite, TiO_2, and many other systems.[18]

Based on the Congo Red dye environmental problem, the main objective of this work is the synthesis and evaluation of TiO_2 photocatalysts with high (001) facets. In this work, we report the synthesis of TiO_2 nanoparticles by a hydrothermal method free of a morphology direction agent, varying the synthesis temperature as a photocatalyst.

Experimental

All chemicals were used as received without further purification and purchased from Sigma-Aldrich. Titanium isopropoxide (TTIP, Ti $[OCH(CH_3)_2]_4$, 97 %), acetic acid (AcOH, $C_2H_4O_2$, 99.7 %), nitric acid (HNO_3, 70 %), Congo Red dye ($C_{32}H_{22}N_6Na_2O_6S_2$, 85 %), sodium hydroxide (NaOH, 97 %), hydrochloric acid (HCl, 37 %), sodium chloride (NaCl, 99 %), miliQ water (H_2O, 18 mΩ).

Synthesis of octahedral TiO_2 nanoparticles photocatalysts.

The synthesis of octahedral TiO_2 nanoparticles was carried out according to Ito et al., with slight variation.[28] In a round-bottom flask, 9.8 mmol of TTIP was added with 11.6 mmol of AcOH, and the flask was put on magnetic agitation for 15 min at room temperature; after that, 0.895 mol of milk water was added and left under fast agitation for 1 h. The next step was to add 3.7 mmol of HNO_3 to the reaction mixture and then place the reaction at 80 °C for 75 min under constant agitation. Finally, after the reaction ended, the mixture was placed in a Teflon flask, introduced into a 125 mL stainless steel autoclave, and left in an oven for 12 h under different reaction temperatures (150, 180, and 210 °C). The resulting colloidal TiO_2 materials were dried in the oven for 24 h at 100 °C.

Characterization of octahedral TiO_2 nanoparticles photocatalysts.

Several techniques were used to characterize the octahedral TiO_2 photocatalysts. The XRD patterns were collected with a Bruker® D8 Advance diffractometer with Cu Kα radiation; the samples were scanned with steps of 0.005 ° and 0.7 s of collection per step. The materials ' BET surface area and pore size distribution were characterized by N_2 adsorption/desorption at 77 K using a Bel-Japan Minisorp II Instrument. TEM analysis was performed with an ARM, JEOL 200F, at an acceleration voltage of 200 kV. Zeta potential as a function of pH was measured by a dynamic light scattering spectrophotometer (Zeta-sizer instrument, Malvern Co., U.K.); the pH of colloidal TiO_2 solution was controlled by HCl (0.1 M) and NaOH (0.1 M) addition.

Photocatalysis test

Photocatalytic degradation experiments were carried out in a photochemical reactor, Rayonet model RPR100, with magnetic stirring. The Congo Red photocatalytic degradation experiments were performed in a cylindrical quartz cell with a reaction volume of 300 cm^3. The Congo Red dye concentration was 25 mg L-1 under UV irradiation at 254 nm at a constant temperature of ~25 °C; the reaction temperature was controlled by solution recirculation in a Liebig condenser. The photodegradation efficiency was determined by plotting C/C_o vs irradiation time (min), where C_o and C are the Congo Red concentration at zero time and time t, respectively. The value of C/C_o was taken as the ratio of A/Ao, i.e., the absorbance value of Congo Red solution at λmax at time t divided by the absorbance at time zero. Congo Red dye exhibits two strong absorption bands at 345 and 497 nm; the intensity absorbance changes were followed by UV-Vis spectroscopy using a Varian model 100 Bio spectrophotometer. Samples of 3 mL were collected from Congo Red solution after a specific time interval and analyzed. To determine the kinetic mechanism for the degradation of Congo red dye in the solution, the pseudo-order model was employed. The apparent rate constant (Kapp) was then determined by

http://dx.doi.org/10.29356/jmcs.v70i1.2436

J. Mex. Chem. Soc. **2026**, *70(1):e2436*
Regular Issue
©2026, Sociedad Química de México
ISSN-e 2594-0317

plotting ln C/C_o versus time during the first 40 min of irradiation, considering that only the variation of Congo red dye concentration vs time, with equation 1.

$$\ln C/C_o = -K_{app}t \qquad \text{Equation 1}$$

Results and discussion

Characterization of octahedral TiO_2 photocatalyst.

X-ray diffraction

X-ray powder diffraction was used to study the crystalline nature and phase purity of octahedral TiO_2 photocatalysts. Fig. 1 shows the XRD patterns of the synthesized octahedral TiO_2 photocatalyst. The diffraction peaks of all samples can be well indexed according to anatase-TiO_2 (JCPDS No. 21-1272), indicating that all products are pure-phase anatase. (101) facets dominate the surface of anatase TiO_2 crystals, and the peak intensity depends on the synthesis temperature. According to Tong et al., the peak intensity ratio of (004) and (101) peaks can establish the preferred orientation of anatase TiO_2 crystals along (001) exposure.[19] Table 1 summarizes the XRD intensity ratio and percentage of 001 facet exposure for the TiO_2 photocatalyst concerning synthesis temperature. Results indicate that TiO_2 photocatalysts with different temperatures preferred orientation along (001) facets, and this orientation increases with increasing synthesis temperature, which agrees with the findings of Liu et al. [20]. However, in this work, the pure anatase TiO_2 phase was synthesized.

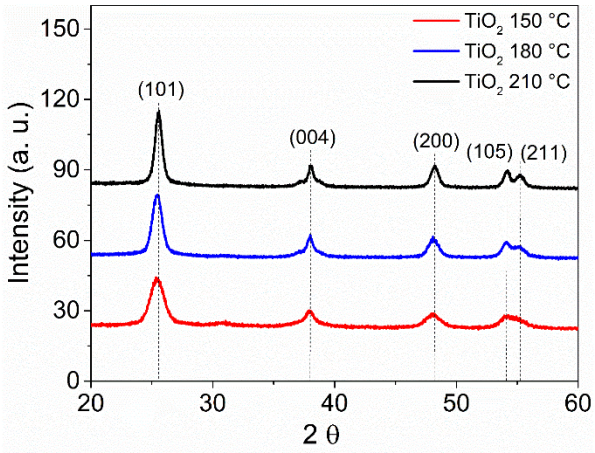

Fig. 1. XRD patterns of TiO_2 photocatalyst.

The crystal size, D, of the samples, was estimated from the full-width at half maximum (β in radians) of the peak at 2θ = 25.4 ° by the Scherrer formula: $D = K\lambda / (\beta \cos \theta)$, K is a constant (0.89), λ is the X-ray wavelength (0.1541 nm for Cu Kα). The crystal sizes of the photocatalysts are presented in Table 1. The results indicate that with temperature increase, the solubility of Ti^{4+} ion is reduced and favored the crystal growth by Ostwald ripening as reported by Kisailus et al., where large crystals grow via ion by ion addition at the expense of small crystals that dissolved into solution inducing an Oriented attachment of (101) and (004) planes increasing the number of (001) facets.[21]

Surface area

Textural properties of the photocatalysts are a measure of available space that molecules would occupy in reactions. The corresponding pore size distribution curves and nitrogen adsorption-desorption isotherm of nitrogen adsorption-desorption isotherms of TiO_2 synthesized photocatalyst are provided in Fig. 2. It can be

http://dx.doi.org/10.29356/jmcs.v70i1.2436

J. Mex. Chem. Soc. **2026**, *70(1):e2436*
Regular Issue
©2026, Sociedad Química de México
ISSN-e 2594-0317

seen that the isotherm is type IV based on the IUPAC classification and one hysteresis loop at a relative pressure range of 0.4-0.8, indicating that TiO_2 photocatalysts mainly consisted of mesopores (type H2).[22]

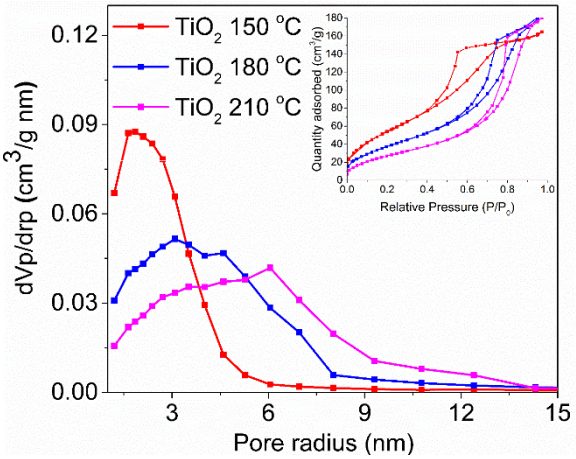

Fig. 2. Distribution of the pore radium and adsorption-desorption isotherm of TiO_2 photocatalyst.

The specific surface area and average pore diameter of the TiO_2 photocatalysts were calculated from the adsorption-desorption isotherms listed in Table 1. The TiO_2 sample synthesized at 150 °C had the highest specific surface area of 207 m^2/g and small pore size, and it is evident by results that hydrothermal temperature during TiO_2 photocatalyst synthesis had a significant effect on their pore structure, crystal size, and crystallinity. The mesopores of TiO_2 photocatalyst samples are from the aggregation of primary particles. However, with temperature increase, the adsorption isotherms shift downward. The hysteresis loops also move to a relatively high-pressure range, indicating the decrease of specific surface areas and the increase of average pore size attributed to the rise of nanoparticle size.[23]

Table 1. Comparison of XRD $I_{(004)}/I_{(101)}$, percentage of {001} facets, Surface area, and pore size of anatase TiO_2 photocatalysts with different synthesis temperatures.

Temperature (°C)	Crystal size (nm)	XRD $I_{(004)}/I_{(101)}$	{001} facets %*	S_{BET} (m^2/g)	Ave. Pore size (nm)
150	5.9	0.40	59	207	3.7
180	8.3	0.38	61	145	7.1
210	11.9	0.31	68	103	12

* The (004)/(101) intensity ratio is an estimation of the (001) facet percentage, and HRTEM confirmed the presence.

Transmission electron microscopy

TEM images determined the shape of TiO_2 nanoparticles, as shown in Fig. 3. These images confirm that the hydrothermal products at different synthesis temperatures are composed of tiny, uniform TiO2 nanocrystals with truncated octahedral bipyramidal shapes, which are promoted by the hydrothermal synthesis temperature. Additionally, the products are free of growth agents, such as HF or polyamine. [24, 25] The high-resolution TEM images from individual nanocrystals show that the fringe spacing of 0.352 nm corresponds to the (101) facets of anatase TiO_2. According to the crystallographic symmetry of anatase TiO_2, the truncated bipyramidal shape is bound by eight (101) planes and two (001) planes. The TiO_2 average nanoparticle size and

http://dx.doi.org/10.29356/jmcs.v70i1.2436

J. Mex. Chem. Soc. **2026**, *70(1):e2436*
Regular Issue
©2026, Sociedad Química de México
ISSN-e 2594-0317

the interplanar spacing of (101) planes were determined from TEM images for all samples and are summarized in Table 2. The increase in nanoparticle size indicates that the growth rate of (001) facets is increased by the synthesis temperature increase, as confirmed by XRD results. The variation in crystal size and nanoparticle size is because TEM measures the overall physical size of individual particles, which may be composed of several crystallites, and XRD measures the size of ordered crystalline regions within a material.

Table 2. Interplanar spacing and average nanoparticle size of TiO_2 photocatalysts.

Samples	**Interplanar spacing (nm)**	**Ave. nanoparticle size (nm) [l×a]**
TiO_2-150 °C	0.355	10.75×6.45
TiO_2-180 °C	0.351	15.35×9.51
TiO_2-210 °C	0.358	17.92×10.18

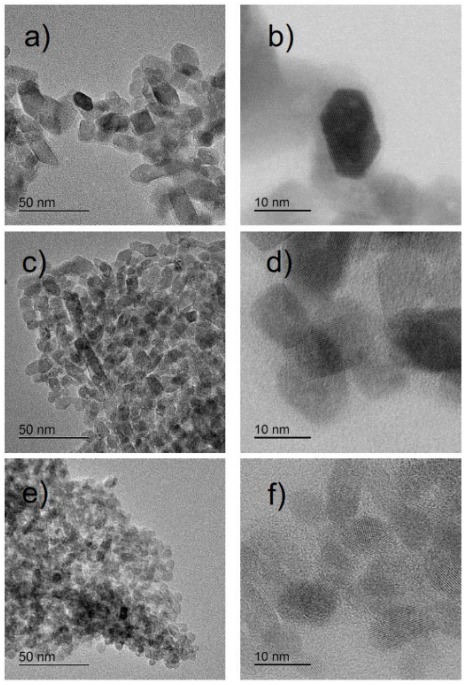

Fig. 3. TEM image of TiO_2 photocatalyst prepared at **(a-b)** 210 °C, **(c-d)** 180 °C, and **(e-f)** 150 °C.

Point of zero charge (PZC) by zeta potential measurements

The PZC of oxide photocatalysts is the pH value at which the surface charge is zero. The knowledge of PZC helps predict whether ion exchange occurs preferentially to specific components of the photocatalyst system, influencing the photocatalytic activity, as well as the stability of photocatalysts by precipitation and solubility. The Zeta potential of TiO_2 photocatalyst synthesized at different temperatures was measured as a function of pH, as shown in Fig. 4. The measurements of zeta potential as a function of final pH showed a correlation with specific surface area; higher specific surface area resulted in lower pzc values.

J. Mex. Chem. Soc. **2026**, *70(1):e2436*
Regular Issue
©2026, Sociedad Química de México
ISSN-e 2594-0317

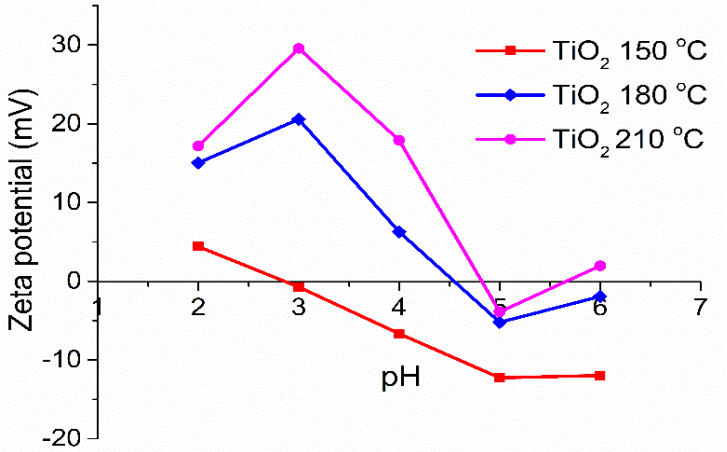

Fig. 4. Zeta potential measurements of TiO_2 photocatalyst.

The pzc values are essential for the photocatalytic experiments in this work, and were carried out at pH 5 and above pH 5.2, the Congo red dye maintains a red-colored solution. The Photocatalyst working near the pzc values, electrostatic repulsion is minimized, leading to particle aggregation and sedimentation, reducing the available surface area for photocatalysis. Far from the PZC, either higher or lower pH, the increased electrostatic repulsion helps to keep particles dispersed, and the photocatalyst can improve the interaction with the pollutant by electrostatic interactions.

Photocatalytic activity

Before the photocatalytic experiment was carried out, the photocatalyst material first adsorbs pollutants from the solution while in darkness. This makes the photocatalyst act as an adsorbent of pollutants, making them more accessible for photocatalytic reaction and leading to complete degradation. In Fig. 5, the dark adsorption of Congo red dye over TiO_2 was carried out for 60 min under constant stirring and UV-Vis measurement, and the results indicate that the adsorption step is carried out within the first 10 min, with a step of equilibrium and a second adsorption step of 10 min. The information obtained from the dark adsorption experiment is crucial for the photocatalytic experiment conducted in this work, which involves 60 min of adsorption followed by starlight irradiation to activate the photocatalyst and promote the oxidation process.

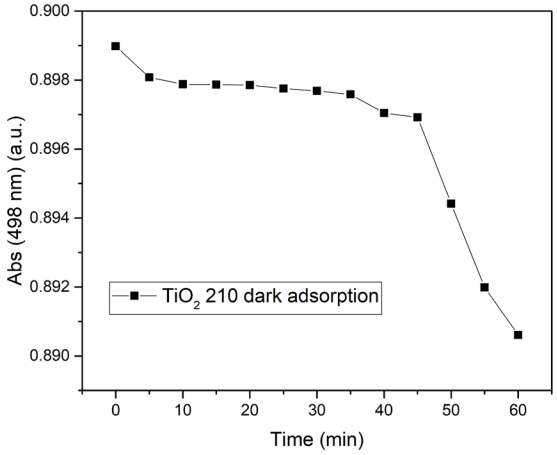

Fig. 5. Dark adsorption of Congo red dye over TiO_2 synthesized at 210 ˚C.

http://dx.doi.org/10.29356/jmcs.v70i1.2436

J. Mex. Chem. Soc. **2026**, *70(1):e2436*
Regular Issue
©2026, Sociedad Química de México
ISSN-e 2594-0317

The photocatalysts efficiency was evaluated in the Congo red dye degradation, studying the synthesis temperature and concentration of the best photocatalysts under UV light at ~25 °C. The CR was selected as a model pollutant because of its extensive use in industrial processes. Three anatase TiO_2 photocatalysts were tested with different exposed (001)/(101) ratios and specific surface areas. Fig. 6 shows the dependencies of the C/C_0 values of the CR solutions at the time of UV light irradiation.

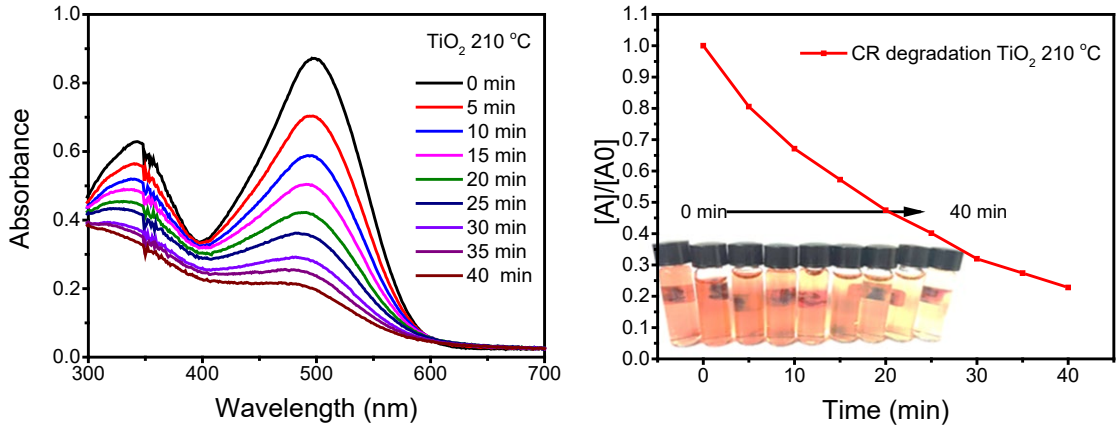

Fig. 6. Photocatalytic performance in the degradation of CR with TiO_2 at 210 °C.

All samples show photocatalytic activity, and Table 3 indicates that photocatalysts with the lowest (001)/(101) ratio present the highest photocatalytic activity and kinetic rate. Results suggest that the exposed (001) facets of anatase TiO_2 nanoparticles are more critical than specific surface area or pore size; however, the number of (001) facets is related to the nanoparticle size or synthesis experimental conditions.

Table 3. Photocatalytic parameter for TiO_2 photocatalysts on CR degradation.

Temperature (°C)	**XRD $I_{(004)}/I_{(101)}$**	**{001} facets %**	**S_{BET} (m^2/g)**	**Photodegradation (%)**	**Kinetic rate $x10^{-3}$ (min^{-1})**
150	0.40	59	207	49.64*	16.8*
180	0.38	61	145	69.84*	30.2*
210	0.31	68	103	77.19*	36.6*

*At 40 min of UV irradiation with 20 ppm of photocatalysts and 25 ppm CR, the kinetics were calculated by the pseudo-first-order model.

As Wei and Wan have reported in their work, the dosage of the photocatalyst can affect the degradation rate. [27] The catalyst dose has a positive and negative impact on the photodecomposition rate, so different concentrations of TiO_2 250 °C photocatalyst in the range of 20 to 40 ppm were employed to study the effect of photocatalyst concentration on the degradation of CR dye, as shown in Fig. 7. Results show that photodegradation efficiency and kinetic rate increase with the increase of catalyst concentration in the range of 20 to 35 ppm, but over this doses a decrease in degradation efficiency took place. An explanation for the observed influence should be that at higher suspended $_{TiO2}$ concentration, more surface area is available in the reaction system. Still, TiO_2 nanoparticles will induce shielding and dispersion of the UV light.

http://dx.doi.org/10.29356/jmcs.v70i1.2436

J. Mex. Chem. Soc. **2026**, *70(1):e2436*
Regular Issue
©2026, Sociedad Química de México
ISSN-e 2594-0317

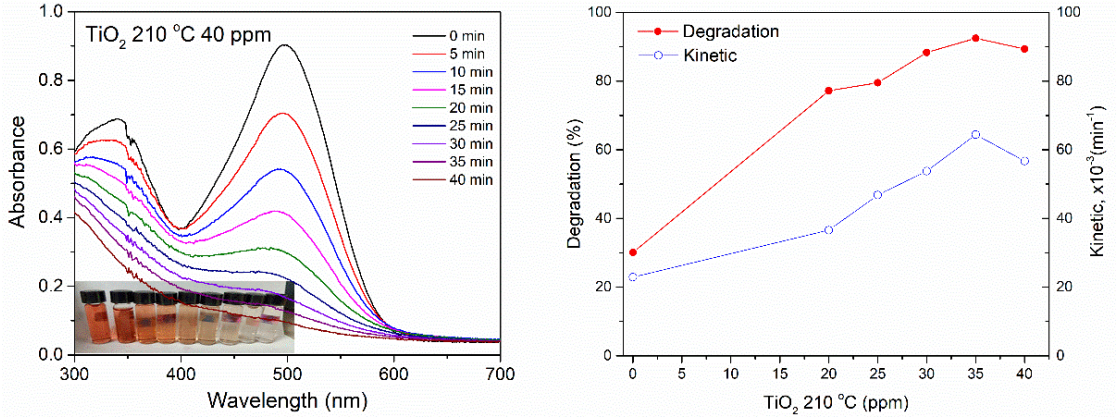

Fig. 7. Effect of TiO_2 210 °C photocatalyst concentration in CR degradation.

Conclusions

In the present research, truncated octahedral bipyramidal TiO_2 nanoparticles were synthesized as photocatalysts by peptization with HNO_3 acid and a hydrothermal method, varying the temperature of the reaction to promote shapes and expose (001)/(101) facets with a ratio variation. Photocatalytic measurements show that the catalyst with the lowest (001)/(101) ratio presents more active sites, like 001 facets, which enhanced the degradation and kinetics of CR photodegradation in 40 min of UV irradiation.

Acknowledgements

We thank the Tecnológico Nacional de México (TecNM), Grant No. 20112.24-P, for supporting this investigation. We also thank Josue E. Romero-Ibarra for TEM technical support at the Laboratorio Universitario de Microscopía Electronica (LUME).

References

1. Tran, H. D.; Nguyen, D. Q.; Do, P. T.; Tran, U. N. P. *RSC Adv.* **2023**, *13*, 16915–16925. DOI: https://doi.org/10.1039/D3RA01970E
2. Reynoso-Soto, E. A.; Pérez-Sicairos, S.; Reyes-Cruzaley, A. P.; Castro-Riquelme, C. L.; Félix-Navarro, R. M.; Paraguay-Delgado, F.; Alonso-Núñez, G.; Lin-Ho, S. W. *J. Mex. Chem. Soc.* **2013**, *57*, 298-305. DOI: https://doi.org/10.29356/jmcs.v57i4.193
3. Thongam, D. D.; Chaturvedi, H. *Nano Express* **2021**, *2*, 12005. DOI: https://doi.org/10.1088/2632-959X/abeb8d
4. Abdelrahman, E. A.; Hegazey, R. M.; Ismail, S. H.; El-Feky, H. H.; Khedr, A. M.; Khairy, M.; Ammar, A. M. *Arab. J. Chem.* **2022**, *15*, 104372. DOI: https://doi.org/https://doi.org/10.1016/j.arabjc.2022.104372
5. Pearson, A.; Jani, H.; Kalantar-zadeh, K.; Bhargava, S. K.; Bansal, V. *Langmuir.* **2011**, *27*, 6661–6667. DOI: https://doi.org/10.1021/la2007765
6. Lee, T.-Y.; Lee, C.-Y.; Chiu, H.-T. *ACS Omega.* **2018**, *3*, 10225–10232. DOI: https://doi.org/10.1021/acsomega.8b01251

J. Mex. Chem. Soc. **2026**, *70(1):e2436*
Regular Issue
©2026, Sociedad Química de México
ISSN-e 2594-0317

7. Liu, X.; Du, G.; Li, M. *ACS Omega.* **2019**, *4*, 14902–14912. DOI: https://doi.org/10.1021/acsomega.9b01648
8. Yang, H. G.; Sun, C. H.; Qiao, S. Z.; Zou, J.; Liu, G.; Smith, S. C.; Cheng, H. M.; Lu, G. Q. *Nature.* **2008**, *453*, 638–641. DOI: https://doi.org/10.1038/nature06964
9. Sun, D.; Yang, W.; Zhou, L.; Sun, W.; Li, Q.; Shang, J. K. *Appl. Catal. B Environ.* **2016**, *182*, 85–93. DOI: https://doi.org/https://doi.org/10.1016/j.apcatb.2015.09.005
10. Liu, G.; Sun, C.; Yang, H. G.; Smith, S. C.; Wang, L.; Lu, G. Q. (Max); Cheng, H.-M. *Chem. Commun.* **2010**, *46*, 755–757. DOI: https://doi.org/10.1039/B919895D
11. Nguyen, C. K.; Cha, H. G.; Kang, Y. S. *Cryst. Growth Des.* **2011**, *11*, 3947–3953. DOI: https://doi.org/10.1021/cg200815t
12. Dinh, C.-T.; Nguyen, T.-D.; Kleitz, F.; Do, T.-O. *ACS Nano.* **2009**, *3*, 3737–3743. DOI: https://doi.org/10.1021/nn900940p
13. Zhao, X.; Jin, W.; Cai, J.; Ye, J.; Li, Z.; Ma, Y.; Xie, J.; Qi, L. *Adv. Funct. Mater.* **2011**, *21*, 3554–3563. DOI: https://doi.org/https://doi.org/10.1002/adfm.201100629
14. Shaban, M.; Abukhadra, M. R.; Ibrahim, S. S.; Shahien, M. G. *Appl. Water Sci.* **2017**, *7*, 4743–4756. DOI: https://doi.org/10.1007/s13201-017-0637-y
15. Saini, D.; Aggarwal, R.; Sonker, A. K.; Sonkar, S. K. *ACS Appl. Nano Mater.* **2021**, *4*, 9303–9312. DOI: https://doi.org/10.1021/acsanm.1c01810
16. Chowdhury, A. P.; Anantharaju, K. S.; Keshavamurthy, K.; Rokhum, S. L. *J. Chem.* **2023**, *2023*, 9780955. DOI: https://doi.org/https://doi.org/10.1155/2023/9780955
17. Harja, M.; Buema, G.; Bucur, D. *Sci. Rep.* **2022**, *12*, 6087. DOI: https://doi.org/10.1038/s41598-022-10093-3
18. Al-Farraj, E. S.; Abdelrahman, E. A. *ACS Omega.* **2024**, *9*, 4870–4880. DOI: https://doi.org/10.1021/acsomega.3c08485
19. Tong, H.; Zhou, Y.; Chang, G.; Li, P.; Zhu, R.; He, Y. *Appl. Surf. Sci.* **2018**, *444*, 267–275. DOI: https://doi.org/https://doi.org/10.1016/j.apsusc.2018.03.069
20. Liu, S.; Yu, J.; Jaroniec, M. *Chem. Mater.* **2011**, *23*, 4085–4093. DOI: https://doi.org/10.1021/cm200597m
21. Kinsinger, N. M.; Wong, A.; Li, D.; Villalobos, F.; Kisailus, D. *Cryst. Growth Des.* **2010**, *10*, 5254–5261.DOI: https://doi.org/10.1021/cg101105t
22. Lee, D.-S.; Lee, S.-Y.; Rhee, K. Y.; Park, S.-J. *Curr. Appl. Phys.* **2014**, *14*, 415–420. DOI: https://doi.org/https://doi.org/10.1016/j.cap.2013.12.018
23. Wang, Z.; Lv, K.; Wang, G.; Deng, K.; Tang, D. *Appl. Catal. B Environ.* **2010**, *100*, 378–385. DOI: https://doi.org/https://doi.org/10.1016/j.apcatb.2010.08.014
24. Nie, S.; Zhao, X.; Liu, B. *RSC Adv.* **2015**, *5*, 103386–103393. DOI: https://doi.org/10.1039/C5RA13006A
25. Liu, N.; Zhao, Y.; Wang, X.; Peng, H.; Li, G. *Mater. Lett.* **2013**, *102–103*, 53–55. DOI: https://doi.org/https://doi.org/10.1016/j.matlet.2013.03.106
26. Li, H.; Vrinat, M.; Berhault, G.; Li, D.; Nie, H.; Afanasiev, P. *Mater. Res. Bull.* **2013**, *48*, 3374–3382.DOI: https://doi.org/https://doi.org/10.1016/j.materresbull.2013.05.017
27. Wei, T. Y.; Wan, C. C. *Ind. Eng. Chem. Res.* **1991**, *30*, 1293–1300. DOI: https://doi.org/10.1021/ie00054a033
28. Ito, S.; Chen, P.; Comte, P.; Nazeeruddin, M. K.; Liska, P.; Péchy, P.; Grätzel, M. *Prog. Photovoltaics Res. Appl.* **2007**, *15*, 603–612. DOI: https://doi.org/https://doi.org/10.1002/pip.768